AGU PUBLICATIONS

JGR

Journal of Geophysical Research: Oceans

RESEARCH ARTICLE

10.1002/2016JC011760

Key Points:
- Statistical analysis of Algerian eddy pathways reveals the barotropic circulation in the region
- Analysis of altimeter data has potential information on subsurface currents and their variability
- Eddy trajectories present a seasonal and interannual variability with three main areas of formation

Correspondence to:
R. Escudier,
rescudier@socib.es

Citation:
Escudier, R., B. Mourre, M. Juza, and J. Tintoré (2016), Subsurface circulation and mesoscale variability in the Algerian subbasin from altimeter-derived eddy trajectories, *J. Geophys. Res. Oceans*, *121*, 6310–6322, doi:10.1002/2016JC011760.

Received 29 FEB 2016
Accepted 3 AUG 2016
Accepted article online 8 AUG 2016
Published online 25 AUG 2016

Subsurface circulation and mesoscale variability in the Algerian subbasin from altimeter-derived eddy trajectories

Romain Escudier[1], Baptiste Mourre[1], Mélanie Juza[1], and Joaquín Tintoré[1,2]

[1]SOCIB, Palma de Mallorca, Spain, [2]IMEDEA (UIB-CSIC), Esporles, Spain

Abstract Algerian eddies are the strongest and largest propagating mesoscale structures in the Western Mediterranean Sea. They have a large influence on the mean circulation, water masses and biological processes. Over 20 years of satellite altimeter data have been analyzed to characterize the propagation of these eddies using automatic detection methods and cross-correlation analysis. We found that, on average, Algerian eddy trajectories form two subbasin scale anticlockwise gyres that coincide with the two Algerian gyres which were described in the literature as the barotropic circulation in the area. This result suggests that altimetry sea surface observations can provide information on subsurface currents and their variability through the study of the propagation of deep mesoscale eddies in semienclosed seas. The analysis of eddy sea level anomalies along the mean pathways reveals three preferred areas of formation. Eddies are usually formed at a specific time of the year in these areas, with a strong interannual variability over the last 20 years.

1. Introduction

Mesoscale eddies are ubiquitous in the global ocean and they dominate the variability of its circulation [*Wyrtki et al*., 1976]. The dynamics of these structures are nonlinear which allow them to transport water across the ocean. They can transport heat content [*Jayne and Marotzke*, 2002; *Colas et al*., 2012] as well as chemical (e.g., salt) and biological properties (e.g., nutrients, biomass [*Feng et al*., 2007; *Llinás et al*., 2009]) over large distances impacting climate [*Wunsch*, 1999] and ecological processes [*Mahadevan et al*., 2012; *McGillicuddy*, 2016]. These structures can also interact with the main currents and affect large scale circulation [*Lozier*, 1997; *Holland*, 1978].

The Algerian subbasin in the south of the Western Mediterranean Sea (WMed) is a highly energetic area of the WMed and is characterized by the presence of large and intense anticyclonic mesoscale eddies. At the surface, the mean circulation is dominated by the Algerian Current, flowing along the African coast at the speed of several tens of centimeters per second. This current is composed of the fresh Atlantic Water (AW) that enters the WMed from the Gibraltar Strait to compensate the deficit of water due to the wind-induced high evaporation.

Below the surface, the general circulation is not well known due to the lack of sufficient in situ observations. Using the trajectories of subsurface Lagrangian floats (at 600, 1200 and 2000 m depth) and deep current meters (at 350, 1000, 1800 m), *Testor et al*. [2005] drew the first picture of the circulation at depth. They described a largely barotropic circulation in the Algerian subbasin consisting of two large anticyclonic gyres, called the Algerian gyres. These gyres follow the f/H contours (f is the planetary vorticity and H the water depth) suggesting that they are constrained by the bathymetry.

Baroclinic instabilities in the Algerian Current causes meanders and eddies [*Millot*, 1987, 1999] that detach from the main flow [*Obaton et al*., 2000]. The large anticyclonic eddies thus formed, known as Algerian Eddies (AEs), have been observed since the 1970s [*Katz*, 1972; *Burkov et al*., 1979]. Available observations (surface drifters, ship CTD campaigns, satellite infrared images, satellite altimetry) have led to the following characterization of these structures. They are large mesoscale vortices of 100–200 km in diameter, with deep vertical signature [*Benzohra and Millot*, 1995]. AEs have been observed to last several months and even several years [*Puillat et al*., 2002]. Uncertainties about the exact vertical extent of these eddies still remain due to the lack of subsurface measurements. Indeed, although many of these eddies have been observed to be quite deep, even reaching the bottom of the ocean at more than 2000 m [*Fuda et al*., 2000;

Ruiz et al., 2002; *Font et al*., 2004], it has also been hypothesized that they could be shallower probably corresponding to the thickness of the Algerian Current of around 200 m [*Millot and Taupier-Letage*, 2005]. A recent study using numerical modeling by *Escudier* [2015] showed that, in average, we could observe anomalies of velocities reaching around 600 m. These baroclinic structures typically present velocities around 50 cm/s at the surface with the intensity of the speed decreasing as we go deeper.

AEs are generated from the Algerian Current along the African coast and propagate downstream at a velocity of a few kilometers per day [*Font et al*., 2004; *Iudicone et al*., 1998] until they detach from the current. Several studies [e.g., *Font et al*., 1998; *Salas et al*., 2002] showed a detachment at 8°E due to the impossibility of crossing the Sardinia Channel. They have been observed to then propagate westward in the center of the Algerian subbasin to close the counterclockwise circuit [*Font et al*., 2004; *Puillat et al*., 2002; *Isern-Fontanet et al*., 2006]. This westward motion has been hypothesized [*Taupier-Letage and Millot*, 1988] to be due to the β-effect on isolated eddies [*Cushman-Roisin et al*., 1990; *McWilliams and Flierl*, 1979] but this would not explain the observed velocities (few millimeters compared to few centimeters per second). Analyzing eddy trajectories from satellite altimetry in the whole Mediterranean, *Isern-Fontanet et al*. [2006] also evidenced some earlier eddy detachment, around 4°E, without obvious explanation.

While they propagate, AEs transport water masses and, for example, are responsible for the spreading of Levantine Intermediate Water (LIW), formed in the eastern Mediterranean, toward the center of the Algerian subbasin [*Fuda et al*., 2000; *Millot and Taupier-Letage*, 2005]. They have an influence on chlorophyll and biological production [*Morán et al*., 2001; *Taupier-Letage et al*., 2003] and play an important role in the mixing of ocean layers [*Isern-Fontanet et al*., 2004]. Due to their size and intensity, they also interact strongly with the Algerian Current and can significantly modify the circulation in the region [*Millot*, 1987; *Taupier-Letage and Millot*, 1988].

Satellite altimetry has demonstrated to be a powerful tool to study mesoscale eddies [*Fu et al*., 2010]. The interpolation of along-track sea level anomalies (SLA) provides weekly to daily maps of surface geostrophic currents over the whole Mediterranean. *Font et al*. [2004] showed that altimetry maps are a useful data set to study AEs. Using an automated eddy detection algorithm, *Isern-Fontanet et al*. [2006] made a statistical study of mesoscale eddies in the Mediterranean Sea. They analyzed the different characteristics of the detected eddies and presented the first description of the trajectory of intense mesoscale eddies with 7 years of altimetry maps. However, the proper characterization of robust propagation pattern was limited by the relative short time series and the characterization of the variability was not addressed. More recently, new studies have successfully applied advanced automated eddy detection methods to the Mediterranean Sea altimeter fields such as *Mkhinini et al*. [2014] and *Escudier et al*. [2016]. *Mkhinini et al*. [2014] have focused on the formation areas of long-lived eddies in the Eastern Mediterranean. *Escudier et al*. [2016], using both altimeter data and a numerical simulation, determined the characteristics such as size, life time, location, periodicity or structure of mesoscale eddies in the WMed.

Taking advantage of the availability of more than 20 years of altimetry maps and the development of advanced eddy detection methods, this paper proposes a more comprehensive analysis of the AE propagation paths and variability. In the section 2, we present the altimetry data set and the eddy detection methods used in this study. Then, in section 3, we compute the mean trajectories of mesoscale eddies from these altimetry maps using two different approaches based on eddy detection methods and cross-correlations of SLA time series. In section 4, we study the spatio-temporal variability of the mesoscale activity along the mean pathways of AEs by analyzing the evolution of SLA along relevant sections of the altimetry maps. Finally, we summarize and discuss the results in section 5.

2. Altimeter Data Analysis

2.1. Gridded Sea Level Anomalies

For this study, we use daily, delayed time gridded maps of SLA in the WMed Sea from AVISO (http://www.aviso.altimetry.fr/duacs/). They are estimated by an optimal interpolation of all available satellite tracks over the period 1993–2014 [*Pascual et al*., 2007]. This product is especially designed for the Mediterranean Sea [*Pujol and Larnicol*, 2005] with a higher resolution grid (1/8°) and smaller correlation scales than the global data set. The along-track data from the satellites are filtered with a Lanczos filter to remove measurement noise (a half-power filter cut-off wavelength of 42 km) and then interpolated with a daily analysis. The

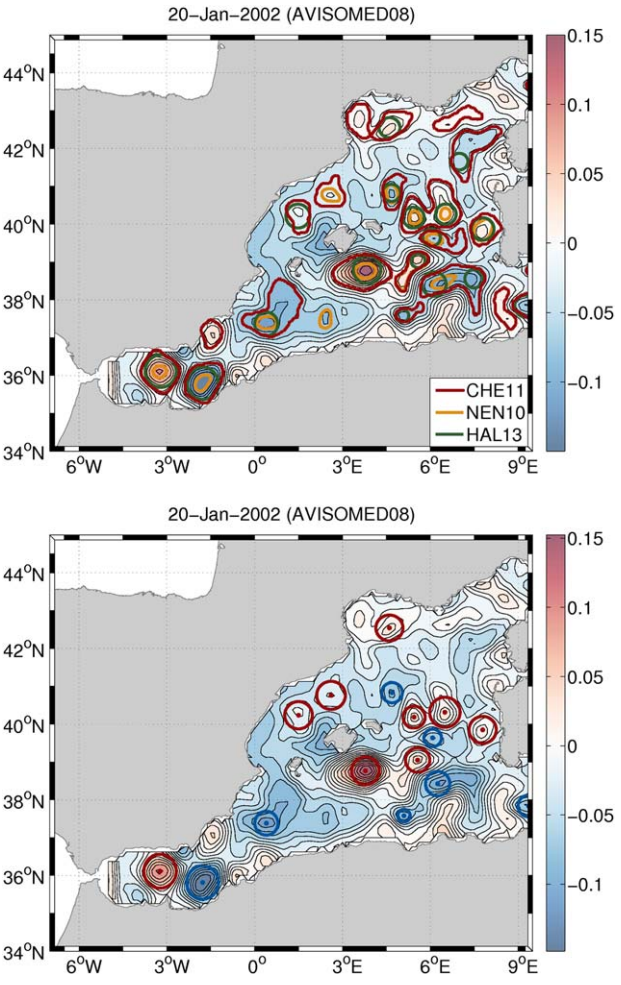

Figure 1. (top) Map of altimetry SLA on 20 January 2002 with eddies detected from the three different methods. the HAL13 method does not provide the shape of the detected eddy so a circle of the eddy radius has been plotted. (bottom) Map of altimetry SLA on 20 January 2002 with cyclones (in blue) and anticyclones (in red) resulting from the combination of the methods.

spatial and temporal correlation scales are constant and set at 100 km and 10 days with a correlation function proposed by *Arhan and De Verdiere* [1985]. The optimal interpolation is set to correct long-wavelength errors and measurement noise. Details of the mapping procedure for the Mediterranean Sea can be found in *Pujol and Larnicol* [2005].

2.2. Eddy Detection and Tracking Algorithm

2.2.1. Detection on Mapped Fields

Many eddy detection methods (EDMs) have been developed in recent years, using different criteria leading to differences in the detected eddies (number, location, size). It is not trivial to determine which method is best suited for our region of study. Since a comparison of these methods is beyond the scope of this study, we decided to apply a combination of three of the most widely used algorithms with the aim of obtaining results that are more robust than those given by a single method.

The first method (CHE11) is described in *Chelton et al*. [2011]. It is a geometry algorithm based on the detection of closed contours of SLA that include a local extremum. The second EDM (NEN10) used is based on the geometry of surface velocities. Explained in *Nencioli et al*. [2010], this method detects points where the velocity field rotates coherently around a center. The third method (HAL13) which is described by *Halo et al*. [2013] combines the geometric criteria similar to the first one with traditional methods based on local deformation properties of the flow such as the Okubo-Weiss parameter [e.g., *Isern-Fontanet et al*., 2006; *Chelton et al*., 2007; *Penven et al*., 2005].

An example of the detection of eddies for one altimetry map in the WMed using the three EDMs is showed in Figure 1 (top). While most of the mesoscale eddies are detected by the different methods, some eddies are detected by only one or two EDMs and some EDMs detect features that are not mesoscale eddies. For example, while the cyclone and anticyclone in the Alboran Sea were detected by all three methods, only two of these algorithms detected eddies in the Balearic Sea. This illustrates the limits of these algorithms in the Mediterranean Sea and justifies the combining approach to obtain more robust results.

The combination of the three methods is based on a very simple protocol: if a structure is detected by only one EDM, it is not considered as an eddy; if it is detected by two or three of the EDMs, it is confirmed as an eddy. The detailed criterion is the following:

1. At least one of the three EDMs has its center inside the disk formed by the center and radius of any of the other. This means that at this position, two EDMs have detected an eddy.
2. The rotation direction must be the same in the different methods that detected the eddy.
3. The position and radius of the detected eddy is defined as the average of the results of the EDMs that detected it.

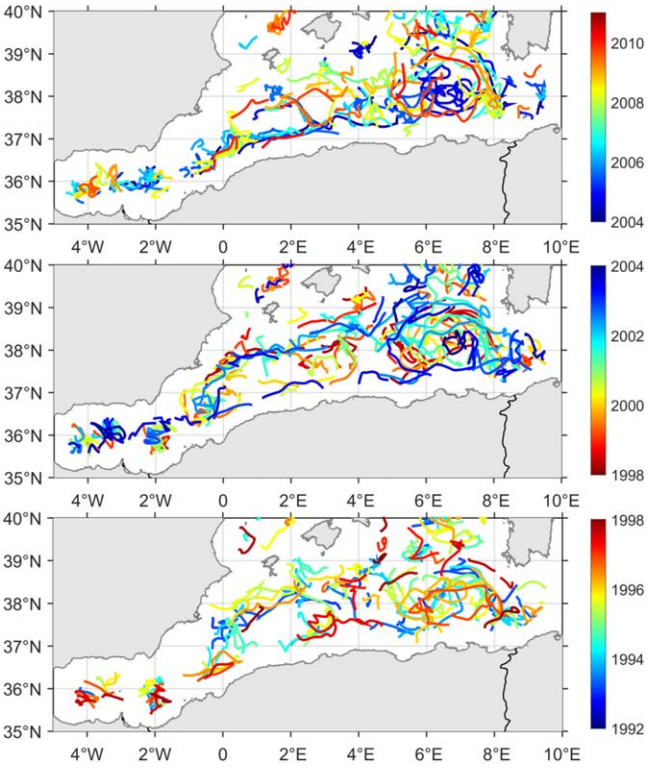

Figure 2. Trajectories of large (radius over 40 km) anticyclonic eddies detected and tracked from altimetry maps for the 20 years period. For clarity, the plot has been separated in three different periods. The color of each trajectory correspond to the year of the starting date of the eddy.

Figure 1 (bottom) shows the resulting eddies detected with the combination of the EDMs. The suspicious eddies that were detected by only one EDM are no longer present and only the robust eddies detected by at least two methods are kept. Once detected, eddies are then tracked in time. For this tracking, to follow an eddy detected at time t, the algorithm searches for the nearest eddy at the following date (t + 1 day) in a circle of 30 km radius. If no surrounding eddy is found, as in *Nencioli et al*. [2010], the search is extended at t + 2 days to account for the algorithm missing the eddy in one map. To ensure that we obtain stable mesoscale eddies, only eddies lasting more than 20 days are kept. In total, around 50,000 eddies are detected by each methods, corresponding to a maximum of detected eddies of 1,50,000. Some of these eddies are the same and thus the combined method is giving a total of 60,000 eddies. Due to unavailability of CHE11 results for the recent years (2013 and 2014), the combined eddy detection method has been applied over the reduced period 1993–2012.

2.2.2. Detection Along One-Dimensional Sections

In section 4, in order to study the spatio-temporal variability of the eddy trajectories, we define sections of altimetry maps along the mean pathways of eddy trajectories, which are previously determined in section 3. To detect eddies along these defined sections, we used an automatic eddy detection on satellite along-track data using wavelet analysis that was developed by *Dussurget et al*. [2011]. The wavelet analysis enables the detection and characterization of nonstationary processes in both time and space [*Torrence and Compo*, 1998]. Assuming a gaussian-like shape of the eddies, a Gaussian wavelet is applied to the section and eddies are detected as local maxima of the scale averaged spectrum.

This method has been successfully applied in the Labrador Sea [*Lilly et al*., 2003], the Bay of Biscay [*Dussurget et al*., 2011] and the Gulf of Mexico [*Le Hénaff et al*., 2014] with altimetry along-track data. Since we are interested in the stable anticyclonic AEs, here again, only eddies lasting more than 20 days have been selected.

3. Characterization of Mean Eddy Pathways

The first step of our analysis consists in characterizing the mean eddy pathways. As mentioned in section 1, several studies in the past have pointed out that AEs are following the Algerian Current before detaching at some point to head northward and then propagate westward. In this section, we will analyze aggregated altimetry maps to investigate this propagation.

3.1. From Automatic Eddy Detection Methods

The combined automated detection and tracking method described in section 2.2 provides the trajectories of mesoscale eddies in the Algerian subbasin. These trajectories are low-pass filtered (cutoff period of 8 days) to remove small variations of the eddy center position due to the algorithm. The large (maximum radius over 40 km) anticyclonic eddy trajectories are presented in Figure 2. Many large anticyclonic

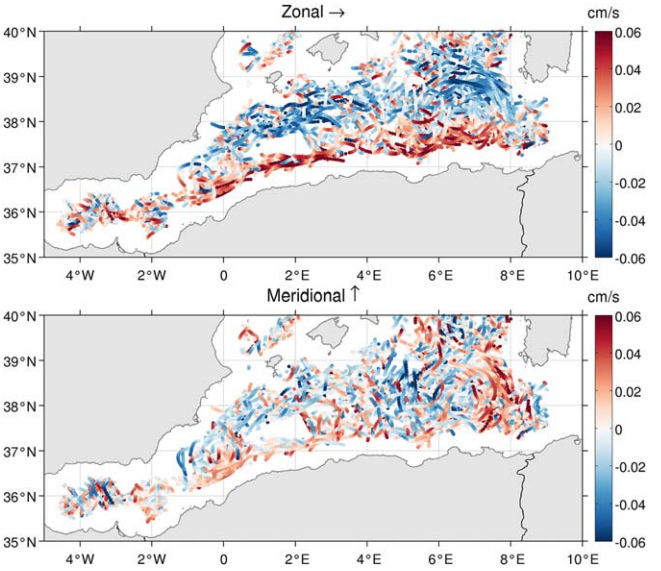

Figure 3. Trajectories of large (radius over 40 km) anticyclonic eddies detected and tracked from altimetry maps for the 20 year period with corresponding (top) zonal and (bottom) meridional velocities.

mesoscale eddies have been detected over the last 20 years, drawing consistent well-defined propagation patterns. In particular, two counterclockwise circulation paths are revealed in this analysis: between 5°E and 8°E and between 1°E and 3–4°E. Eddies detected west of 1°W are quasi static around 4°W and 2°W and correspond to variation in intensity of the two Alboran gyres [*Renault et al.*, 2012].

To further examine this behavior, we compute Lagrangian velocities of the eddies from their trajectories. These zonal and meridional eddy propagation velocities are indicated in Figure 3 as the dot color of the eddy trajectories. The plot of zonal velocities shows a clear eastward propagation along the Algerian coast with velocities from 3 to 6 cm/s and westward propagation in the northern part of the circulation at a similar pace. The meridional velocities plot highlights the detachment and northward propagation of the AEs that were situated along the Algerian coast occurring between 2.5°E and 4°E and around 8°E. It also reproduces the southward propagation around 0°E and 5°E from the northern part to the southern part of the circulation.

From these eddy propagation speeds along the trajectories, we compute the mean velocity in boxes of 1/3° x 1/3° separating cyclonic and anticyclonic eddies. Figure 4 shows the resulting maps of mean propagation speed. The top plot relative to anticyclones depicts the two anticlockwise gyres as clear paths of preferred eddy propagation. These gyres coincide with the Algerian gyres documented by *Testor et al.* [2005], which characterize the barotropic circulation in the Algerian subbasin. The position (centered at around 2°E and 7°E), size (several hundreds of km) of the gyres in this map match the description resulting from the analysis of subsurface drifting buoys in *Testor et al.* [2005]. The details of the interaction between mesoscale baroclinic eddies and oceanic currents are certainly very complex [e.g., *Marshall and Parthasarathy*, 1993; *Vandermeirsch et al.*, 2001, 2002]. However, *Vandermeirsch et al.* [2001] showed that the propagation of eddies could be mainly attributed to the combination of the planetary beta-effect and the advection by the barotropic part of the large-scale flow, the baroclinic flow having a very limited influence on the vortex translation in their experiments. This finding was confirmed by several studies analyzing the

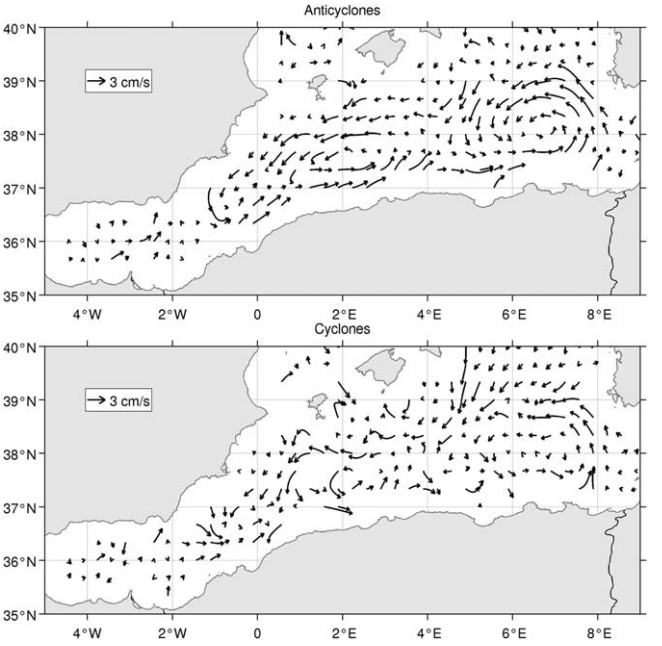

Figure 4. Average velocities of anticyclonic (top) and cyclonic (bottom) eddies in boxes of 1/3° × 1/3°.

propagation of ocean mesoscale eddies in different parts of the world affected by significant barotropic currents. The propagation speed was found to be close to the westward motion due to the β-effect doppler-shifted by the surrounding current [*Fu*, 2006; *Fu et al*., 2009; *Chelton et al*., 2011; *Klocker and Marshall*, 2014]. The westward drift can be approximated as $V_b = -\beta R_d^2$ for large eddies [*McWilliams and Flierl*, 1979] with R_d, the Rossby internal radius of deformation. In the region, $R_d = 15$ km, and $\beta = 1.8 * 10^{-11}$ for 38°N which gives $V_b = 0.4$ cm/s. If we consider the westward drift of an isolated anticyclone in a reduced-gravity shallow-water model [*Nezlin and Sutyrin*, 1994; *Stegner and Zeitlin*, 1996], nonlinear effects induced by the finite isopycnal deviation may lead to a supercritical drift speed of $V_{drift} = V_b(1 + a * R_o * (R/R_d)^2)$, where R_o is the Rossby number and a is a geometrical factor that depends on the eddy shape. For the AE anticyclones, if we take a = 1 in the first approximation, with $R_o = 0.1$ and $R = 50$ km, V_{drift} is then equal to 0.8 cm/s, the double of V_b. Removing this effect to the values of deep currents obtained by *Testor et al*. [2005], we obtain an intensity of around 4 cm/s along the Algerian coast and 3.5 cm/s for the northern part of the gyres (from values of respectively 5 and 2.5 cm/s found with moored current meters). These values are very close, albeit a little higher, than the values (around 3 cm/s) of the velocities presented in figure 4. The vertical extension of these eddies, down to many hundreds of meters if not the ocean floor, make them sensitive to the advection by integrated currents over a significant depth. Our results suggest that the circulation of anticyclonic AEs is consistent with the barotropic circulation in the Algerian basin. The impact of the integrated current on the propagation of mesoscale eddies has similarly been observed by *Fu* [2006] in the south west Atlantic. Regarding cyclones (Figure 4, bottom), even if they are somehow advected along these gyres, the resulting circulation is less clear than for anticyclones. This is very likely due to the fact that cyclones are shallower (few hundreds of meters) in this region [*Escudier et al*., 2016] and therefore less affected by the subsurface currents. Our interpretation is that the wind, the surface currents and interaction with other eddies may significantly impact their trajectories which do not lead to a well-defined averaged propagation pattern.

3.2. From Cross-Correlation Analysis

The previous method highlights a robust mean circulation pattern of mesoscale eddies following the shape of the barotropic Algerian gyres. However, it relies on some assumptions about the eddies, selecting large anticyclones, and about the parametrization of eddy detection methods. We applied another statistical method that does not require any previous assumption to confirm these results.

More specifically, we use cross-correlations of the SLA time series over the period 1993–2014 to determine the mean eddy pathways. As a first approach, we present in Figure 5 the lagged cross-correlation between the time series of SLA averaged in several spatial boxes and the time series at each grid point. A color is assigned for each box and the patch of color corresponds to the area, at a given time lag, of significant correlation with the time series in the box. The figure presents three different lags (−40, 0, and 40 days) for nine boxes. The correlation patch for the boxes 2, 3, 4 and 5 travel eastward with time which corresponds to the bottom part of the Algerian gyres. The anticlockwise rotation associated with the eastern Algerian gyre is revealed by the correlations corresponding to boxes 5, 6, 7 and 8. Box 9 shows the westward propagation in the northern part of the western Algerian gyre. Almost no propagation is found for box 1 in the eastern Alboran Sea which is consistent with the trajectories of eddies observed in Figure 2 and with the literature describing the static Eastern Alboran gyre [*Renault et al*., 2012].

Figure 5 illustrates how the cross-correlation patches give relevant information on the propagation of anomalies of sea surface height due to mesoscale eddies. To be able to estimate propagation velocities we focus on the trajectory of the maximum of this patch following the method described in *Fu* [2009]. This allows to plot an averaged map as in the previous section. The method relies on the detection of the position of the correlation maximum at different lags for regular boxes of 1/3° x 1/3°. Then, the lagged velocities for one box are computed by dividing the distance between the time-lagged maximum and the center of the box by the time lag. The final velocity for the box is the correlation weighted average of the lagged velocities. We applied the same protocol with a maximum lag of 15 days and maximum distance of 150 km which are suited to our study area. Sensibility test on the values of these parameters have not showed any significant impact. The results, presented in Figure 6, allow the quantification and visualization of the mean propagation velocities. It again evidences two main anticlockwise propagation patterns corresponding to the documented barotropic Algerian gyres. The gyres are less pronounced than in Figure 4 as we are not

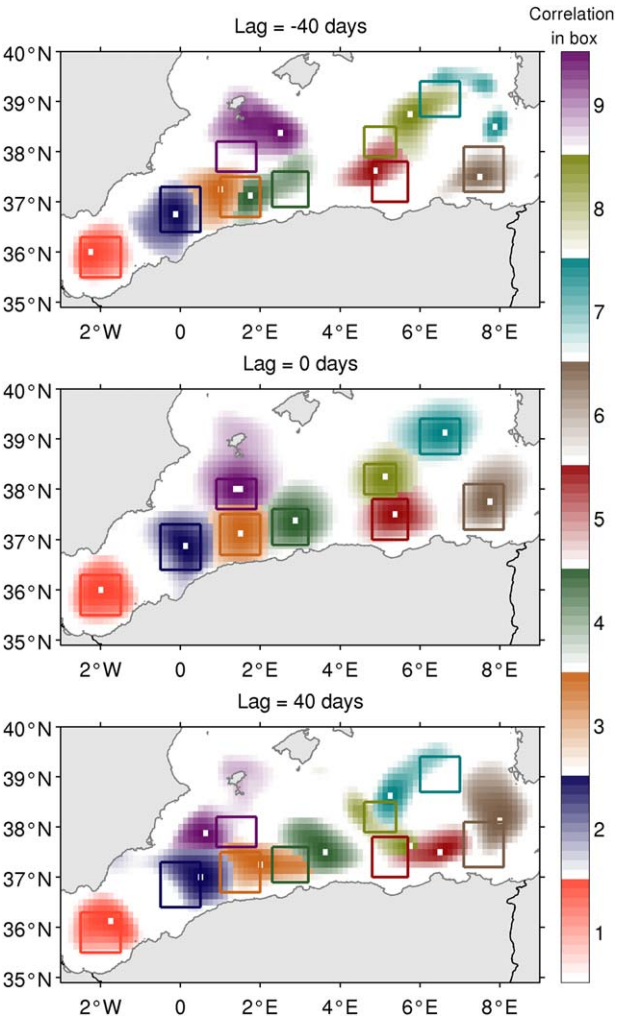

Figure 5. Cross correlation between the time series of SLA in different boxes and the other grid points at different lags. The nine boxes are indicated and each box has a different color. In the background, the significant values at 99% of the correlation for each of the boxes are plotted in shade of the color corresponding to the box, white corresponding to no correlation and the box color correspond to the maximum correlation at this lag. The white point marks the position of the maximum of correlation for each box. If there is a point where there is significant correlation for two different boxes, the color for the box with higher correlation is chosen.

selecting large, long-lived anticyclones but instead considering any SLA structure. The propagation velocity from this analysis is around 3 cm/s.

4. Spatiotemporal Variability

Both the automatic eddy detection method and the statistical cross-correlation analysis have shown the existence of defined propagation paths of AEs. Focusing along these paths, we are now able to study the spatial and temporal variability of eddy propagation using Hovmöller diagrams, which display the evolution of SLA along a section. The sections used to compute the Hovmöller are presented in Figure 7. They correspond to the different mean pathways highlighted in section 3. According to the results of section 3, eddies generated in the western part of the Algerian subbasin are advected along the section 1 until they reach 4°E where they can either head northward along the section 3 rotating around the western Algerian gyre or keep on traveling eastward and enter the eastern Algerian gyre along the section 2. To detect large anticyclonic eddies and remove some of the noise from small structures and altimeter errors, each section is defined as a band (see Figure 7) and the value of SLA is averaged over the width of the band.

We analyze the whole available period of altimetry (1993–2014) in this paper but we initially focus on the period 2009–2014 (Figure 8) for an easier description of the Hovmöller. Red patches on the figure correspond to the propagation of AEs along the pathways defined in Figure 7. The automatic detection of eddies on satellite along-track data using wavelet analysis (described in section 2) has been adapted and applied to the Hovmöller sections. The resulting detected large and long-lived anticyclones are indicated in green on the figure.

Several large anticyclonic eddies are formed in the first section and propagate eastward (in 2010, 2012, and 2013). The slow propagation until point 2 (1 cm/s) is in agreement with the mean velocities plots estimated in Figures 4 and 6. After that, the propagation speed of the eddies is around several km per day (3–4 cm/s) as described in the literature. Some of the anticyclones continue propagating eastward and are detected in section 2 where they rotate around the eastern gyre (e.g., beginning of 2013 and 2014). Some eddies are formed between point 3 and 4 in section 2, which corresponds to 6°E, and then are advected as the other eddies around the gyre (e.g., beginning of 2009 or mid-2011). In section 3, the western propagation of some AEs is depicted but they are fewer of them (mid-2009 and 2011).

The three Hovmöller diagrams for the whole 22 year period are presented in Figure 9. It shows the interannual variability of the AEs formation and propagation. Around 20 large AEs are detected in the first section

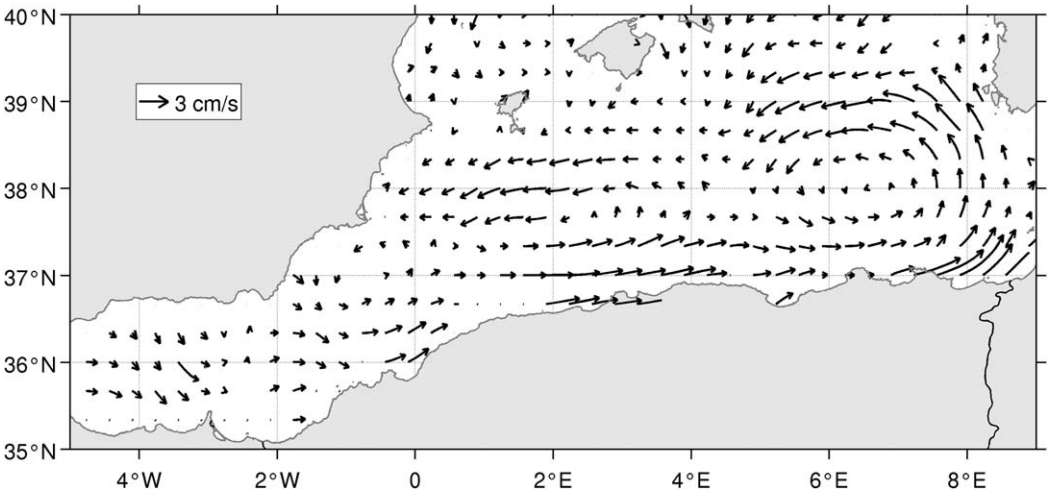

Figure 6. Averaged velocities of mesoscale eddies estimated from cross-correlation maximum method in boxes of 1/3°x1/3°.

in the last 20 years, 80 in the second section and 25 in the third section. The large eddies in section 1 are formed quite regularly with 6 months to 2 years intervals.

As shown in Figure 9, AEs tend to appear at the same month of the year. To examine this aspect, we plot in Figure 10 the annual climatology of the SLA over the same sections. It shows that, on average, in section 1, eddies are generated at 1°W (beginning of the Hovmöller) in December-January and then propagate during the year until next December and around point 2. There, they accelerate and travel eastward to reach at 4°E mid-February where they loop back on section 3 until August-September. In April, additional eddies are generated at 2°E and propagate eastward toward 4°E in June-July where they either follow the same loop back through section 3 as the one in February or head eastward in section 2 to loop around the eastern Algerian gyre in 1 year.

As evidenced in the Hovmöller diagrams, there are different formation areas for the AEs. On Figure 11, the distribution of the starting points of the detected trajectories along the section off the Algerian coast is presented. Three main formation areas can be identified. First, the strongest one is situated between 2°W and 1°W and is the formation area of eddies propagating eastward along the whole section 1. Then, between 1°E and 3°E, there is a weaker area of eddy formation as already pointed out on the Hovmöller of interannual and climatological SLA. The last one, between 6°E and 7°E is on the eastern part of the eastern Algerian gyre and generates eddies that either stay in this position or detach northward to recirculate around the western Algerian gyre.

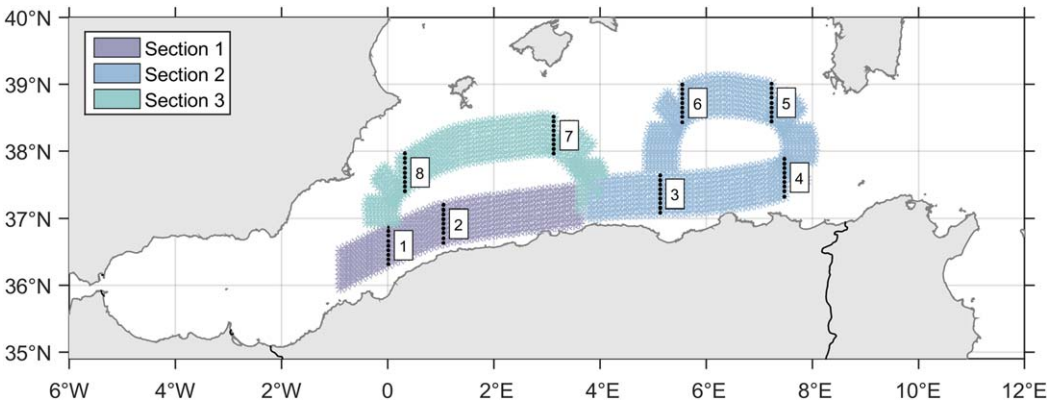

Figure 7. Sections used for the Hovmöller diagrams. Relevant positions for the analysis have been indicated and numbered.

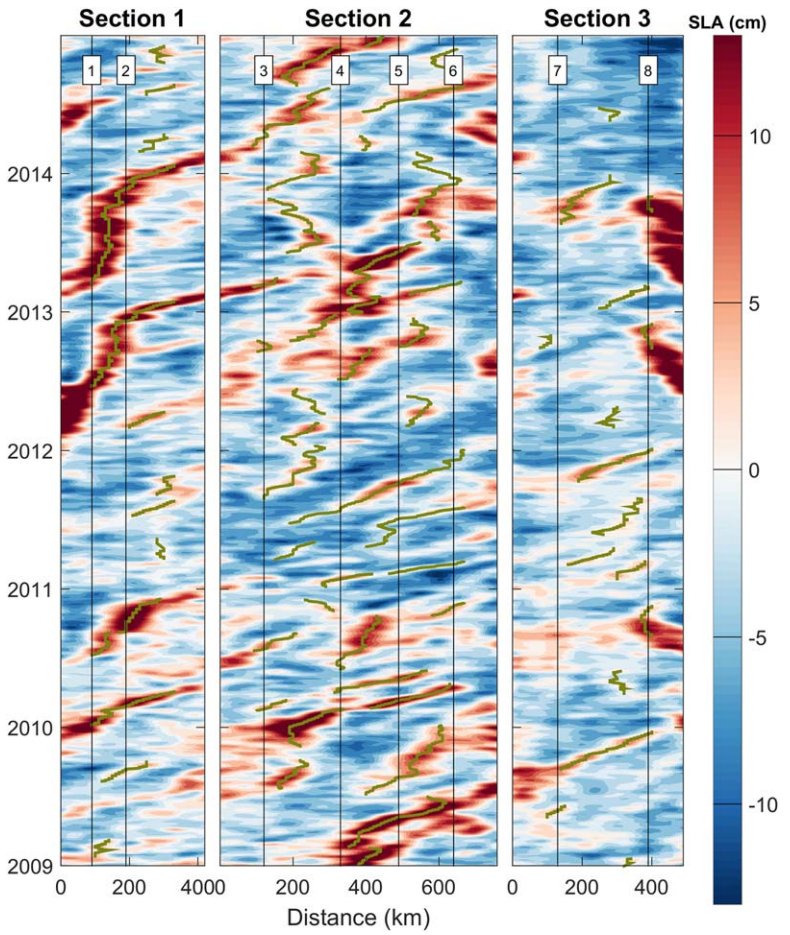

Figure 8. Hovmöller diagrams of SLA for the period 2009–2014 along the sections defined in figure 7 with relevant positions indicated with their number. Large and intense detected anticyclones are depicted in green.

5. Discussion

Using 20 years of merged altimetry SLA maps, we were able to determine the mean pathways of AEs. To accomplish this, we used two different methods to compute the mean velocities of eddies in the region. In the first one (lagrangian), we computed these velocities with the trajectory of mesoscale eddies obtained from eddy detection methods. In the second one (eulerian), we employed a different statistical method that computes the trajectory of the maximum of cross-correlation. Both methods led to the same results: in the region, mesoscale eddies follow two anticlockwise gyres which coincide with the two large Algerian gyres that characterize the circulation of the subsurface layers as described by *Testor et al*. [2005] using subsurface drifters and current meters. Since the Algerian gyres appear to be constrained by the f/H contours [*Testor et al*., 2005], ultimately eddy trajectories are constrained by the bathymetry of the region.

This result somehow contradicts the previous assumptions of eddies advected along the Algerian Current in the southern part of the basin with a return travel westward in the northern part due to the β-effect. It is certainly explained by the vertical extent of these eddies, most of which reach more than 1000 m and it indicates that these eddies are sensitive to the depth-averaged currents over a large part of the water column. This mechanism accounts for the propagation velocities of the eddies (3 cm/s) that are an order of magnitude weaker than the surface Algerian Current (several tens of centimeters per second) and an order of magnitude higher than the propagation by the β-effect (few millimeters per second). They are actually very similar to the values observed of the subsurface currents (5 cm/s in the Algerian current and 2–3 cm/s in the northern part [*Testor et al*., 2005]) after removing the eddy intrinsic propagation due to beta-effect. It also gives an explanation for the detachment and return circulation of the AEs.

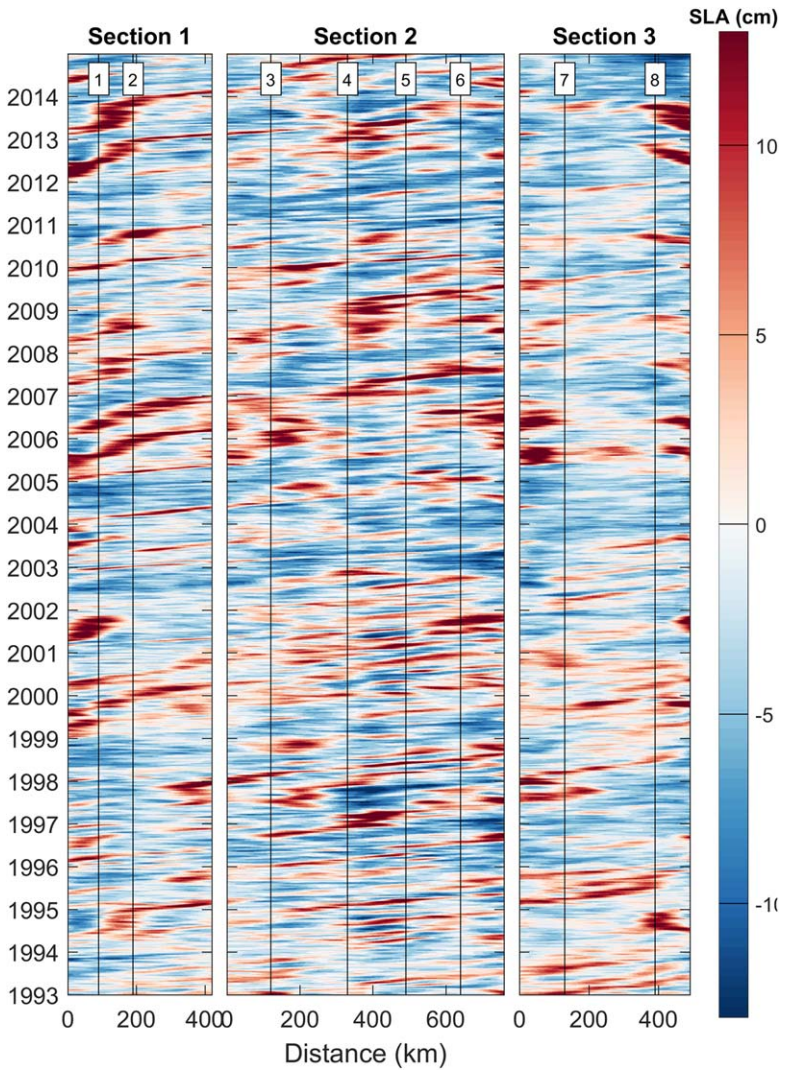

Figure 9. Hovmöller diagrams of SLA for the period 1993–2014 along the sections defined in figure 7 with relevant positions indicated with their number.

As stated above, large anticyclonic eddies in the region have deep vertical extensions that make them sensitive to the depth-integrated currents. In the Algerian subbasin, we hypothesize that this is the reason why the trajectories of cyclones, which are shallower, do not give such a clear picture of the subsurface circulation. This study indicates that a sufficient number of AEs are deep enough to be advected by depth-integrated currents. Further studies should be carried out to confirm these indications and identify the underlying mechanisms, in particular allowing to distinguish between the effect of the mean flow and that of the bottom topography. Numerical modeling could be a useful tool to explore these interactions.

Importantly, one of the implications of our study is that altimeter sea surface observations might provide insights into subsurface circulation through the analysis of the propagation of these mesoscale eddies. This may allow the monitoring of subsurface currents, of which we generally have very limited observations, and the study of the associated interannual to decadal and climatic variability. Indeed, in the Algerian subbasin, the few subsurface drifters trajectories and current meters measurements that enabled the first description of the Algerian gyres by *Testor et al*. [2005] are the only documented subsurface velocity observations.

In the Algerian subbasin, we plotted Hovmöller diagrams along the preferred pathways of the eddies that we inferred from the maps of mean propagation speed. These diagrams show that the large anticyclonic

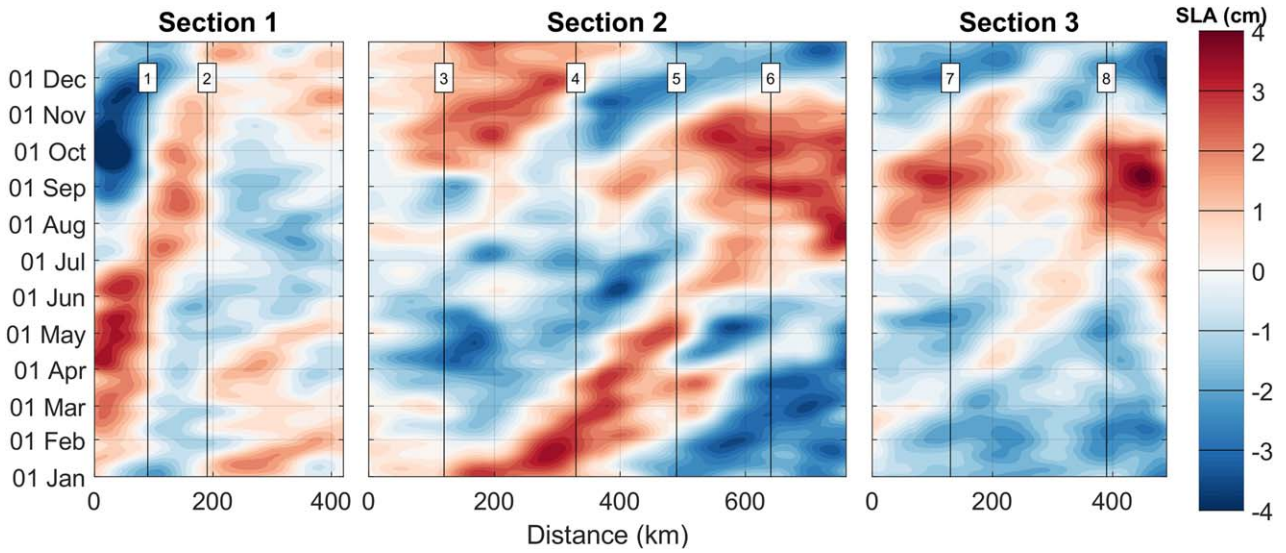

Figure 10. Annual climatology of the SLA for the period 1993–2014 along the sections indicated in figure 7 with relevant positions indicated with their number.

AEs are formed regularly in three different areas along the Algerian coast. Notably, the ones generated between 1°W and 2°W appear almost every year or every other year. The eddies formed in this region first propagate slowly eastward then accelerate to circulate around one or the other gyre. The other areas of formation are situated inside the gyres. The formation and propagation time of the AEs have been studied with a climatology of the Hovmöller diagrams which show preferred time of the year for the propagation paths.

These results have implications on the estimation of the transport of water masses, heat and biology through the AEs. For example, the monitoring of AEs propagation directly helps the estimation of the LIW transport in the Western Mediterranean basin since the AEs have been shown to be responsible for the spreading of LIW in the central basin. AEs also have key role in the transfer of matter at basin scale [*Gorsky et al.*, 2002; *Taupier-Letage et al.*, 2003] and therefore characterizing their variability is essential to properly evaluate their impact.

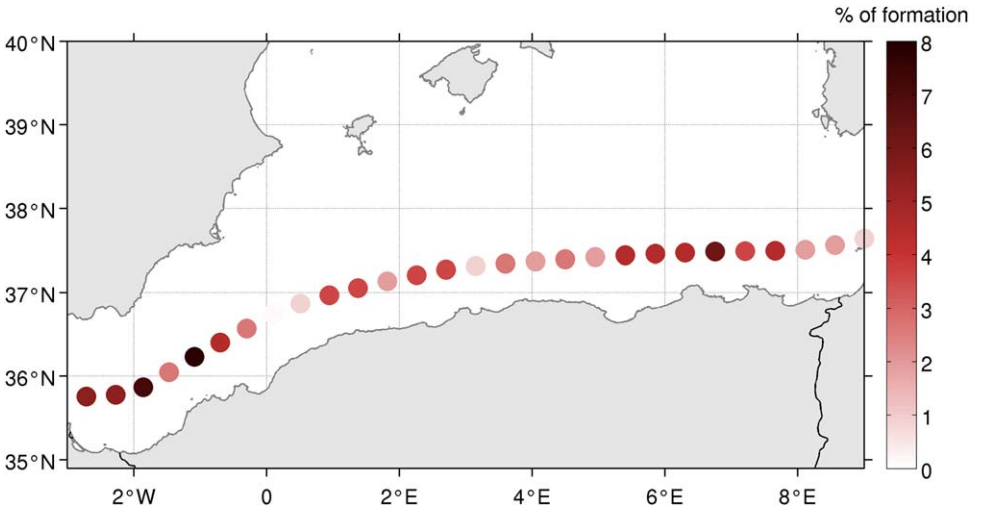

Figure 11. Distribution of formation points of 165 anticyclonic eddies detected on the Hovmöller diagram of the section along the Algerian coast.

Acknowledgments
This work was supported by LaCaixa fundation through the MedClic project. The SLA data were generated by DUACS and distributed by AVISO (ftp://ftp.aviso.oceanobs.com). The eddy detection results for the period 1992–2010 may be obtained from Romain Escudier (email: rescudier@socib.es). The authors want to thank the reviewer and editor for their insightful and constructive comments on the paper.

References

Arhan, M., and A. C. De Verdiere (1985), Dynamics of eddy motions in the eastern North Atlantic, *J. Phys. Oceanogr.*, *15*(2), 153–170.
Benzohra, M., and C. Millot (1995), Hydrodynamics of an open sea Algerian eddy, *Deep Sea Res., Part I*, *42*(10), 1831–1847.
Burkov, V., V. Krivosheya, I. Ovchinnikov, and M. Savin (1979), Eddies in the current system of the western Mediterranean Sea, *Oceanology*, *19*(1), 9–13.
Chelton, D. B., M. G. Schlax, R. M. Samelson, and R. A. de Szoeke (2007), Global observations of large oceanic eddies, *Geophys. Res. Lett.*, *34*, L15606, doi:10.1029/2007GL030812.
Chelton, D. B., M. G. Schlax, and R. M. Samelson (2011), Global observations of nonlinear mesoscale eddies, *Prog. Oceanogr.*, *91*(2), 167–216.
Colas, F., J. C. McWilliams, X. Capet, and J. Kurian (2012), Heat balance and eddies in the peru-chile current system, *Clim. Dyn.*, *39*(1-2), 509–529.
Cushman-Roisin, B., B. Tang, and E. P. Chassignet (1990), Westward motion of mesoscale eddies, *J. Phys. Oceanogr.*, *20*(5), 758–768.
Dussurget, R., F. Birol, R. Morrow, and P. D. Mey (2011), Fine resolution altimetry data for a regional application in the Bay of Biscay, *Mar. Geod.*, *34*(3-4), 447–476.
Escudier, R. (2015), Mesoscale eddies in the western Mediterranean Sea: Characterization and understanding from satellite observations and model simulations, PhD thesis, Univ. de les Illes Balears, Spain and Univ. de Grenoble, France.
Escudier, R., L. Renault, A. Pascual, P. Brasseur, D. Chelton, and J. Beuvier (2016), Eddy properties in the western Mediterranean Sea from satellite altimetry and a numerical simulation, *J. Geophys. Res. Oceans*, *121*, 3990–4006, doi:10.1002/2015JC011371.
Feng, M., L. J. Majewski, C. Fandry, and A. M. Waite (2007), Characteristics of two counter-rotating eddies in the leeuwin current system off the western Australian coast, *Deep Sea Res., Part II*, *54*(8), 961–980.
Font, J., C. Millot, J. Salas, A. Julia, and O. Chic (1998), The drift of modified Atlantic water from the Alboran sea to the eastern Mediterranean Sea, *Sci. Mar.*, *62*(3), 211–216.
Font, J., J. Isern-Fontanet, and J. De Jesus Salas (2004), Tracking a big anticyclonic eddy in the western Mediterranean Sea, *Sci. Mar.*, *68*(3), 331–342.
Fu, L.-L. (2006), Pathways of eddies in the South Atlantic Ocean revealed from satellite altimeter observations, *Geophys. Res. Lett.*, *33*, L14610, doi:10.1029/2006GL026245.
Fu, L.-L. (2009), Pattern and velocity of propagation of the global ocean eddy variability, *J. Geophys. Res.*, *114*, C11017, doi:10.1029/2009JC005349.
Fu, L.-L., D. Alsdorf, E. Rodriguez, R. Morrow, N. Mognard, J. Lambin, P. Vaze, and T. Lafon (2009), The swot (surface water and ocean topography) mission: Spaceborne radar interferometry for oceanographic and hydrological applications, in Proceedings of the "OceanObs'09: Sustained Ocean Observations and Information for Society" Conference (Vol. 2), Venice, Italy, 21–25 September, edited by J. Hall, D. E. Harrison and D. Stammer, ESA Publication WPP-306, 2010.
Fu, L.-L., D. B. Chelton, P.-Y. Le Traon, and R. Morrow (2010), Eddy dynamics from satellite altimetry, *Oceanography*, *23*(4), 14–25.
Fuda, J., C. Millot, I. Taupier-Letage, U. Send, and J. Bocognano (2000), Xbt monitoring of a meridian section across the western Mediterranean Sea, *Deep Sea Res., Part I*, *47*(11), 2191–2218.
Gorsky, G., L. Prieur, I. Taupier-Letage, L. Stemmann, and M. Picheral (2002), Large particulate matter in the western Mediterranean: I. *LPM distribution related to mesoscale hydrodynamics, J. Mar. Syst.*, *33*, 289–311.
Halo, I., B. Backeberg, P. Penven, I. Ansorge, C. Reason, and J. Ullgren (2013), Eddy properties in the mozambique channel: A comparison between observations and two numerical ocean circulation models, *Deep Sea Res., Part II, 100*, 38–53.
Holland, W. R. (1978), The role of mesoscale eddies in the general circulation of the ocean-numerical experiments using a wind-driven quasi-geostrophic model, *J. Phys. Oceanogr.*, *8*(3), 363–392.
Isern-Fontanet, J., J. Font, E. García-Ladona, M. Emelianov, C. Millot, and I. Taupier-Letage (2004), Spatial structure of anticyclonic eddies in the Algerian basin (Mediterranean Sea) analyzed using the Okubo–Weiss parameter, *Deep Sea Res., Part II*, *51*(25), 3009–3028.
Isern-Fontanet, J., E. García-Ladona, and J. Font (2006), Vortices of the Mediterranean Sea: An altimetric perspective, *J. Phys. Oceanogr.*, *36*(1), 87–103.
Iudicone, D., R. Santoleri, S. Marullo, and P. Gerosa (1998), Sea level variability and surface eddy statistics in the Mediterranean Sea from TOPEX/POSEIDON data, *J. Geophys. Res.*, *103*(C2), 2995–3011.
Jayne, S. R., and J. Marotzke (2002), The oceanic eddy heat transport., *J. Phys. Oceanogr.*, *32*(12), 3328–3345.
Katz, E. J. (1972), The levantine intermediate water between the Strait of Sicily and the Strait of Gibraltar, *Deep Sea Res. Oceanogr. Abstr.*, *19*, 507–520.
Klocker, A., and D. P. Marshall (2014), Advection of baroclinic eddies by depth mean flow, *Geophys. Res. Lett.*, *41*, 3517–3521, doi:10.1002/2014GL060001.
Le Hénaff, M., V. H. Kourafalou, R. Dussurget, and R. Lumpkin (2014), Cyclonic activity in the eastern Gulf of Mexico: Characterization from along-track altimetry and in situ drifter trajectories, *Prog. Oceanogr.*, *120*, 120–138.
Lilly, J. M., P. B. Rhines, F. Schott, K. Lavender, J. Lazier, U. Send, and E. D'Asaro (2003), Observations of the Labrador Sea eddy field, *Prog. Oceanogr.*, *59*(1), 75–176, doi:10.1016/j.pocean.2003.08.013.
Llinás, L., R. S. Pickart, J. T. Mathis, and S. L. Smith (2009), Zooplankton inside an Arctic Ocean cold-core eddy: Probable origin and fate, *Deep Sea Research Part II: Topical Studies in Oceanography*, *56*(17), 1290–1304.
Lozier, M. S. (1997), Evidence for large-scale eddy-driven gyres in the North Atlantic, *Science*, *277*(5324), 361 –364, doi:10.1126/science.277.5324.361.
Mahadevan, A., E. D'Asaro, C. Lee, and M. J. Perry (2012), Eddy-driven stratification initiates North Atlantic spring phytoplankton blooms, *Science*, *337*(6090), 54–58.
Marshall, J., and B. Parthasarathy (1993), Tearing of an aligned vortex by a current difference in two-layer quasi-geostrophic flow, *J. Fluid Mech.*, *255*, 157–182.
McGillicuddy, D. (2016), Mechanisms of physical–biological–biogeochemical interactions at the oceanic mesoscale, *Annu. Rev. Mar. Sci.*, *8*, 13–1.
McWilliams, J. C., and G. R. Flierl (1979), On the evolution of isolated, nonlinear vortices, *J. Phys. Oceanogr.*, *9*(6), 1155–1182.
Millot, C. (1987), Circulation in the western Mediterranean-Sea, *Oceanol. Acta*, *10*(2), 143–149.
Millot, C. (1999), Circulation in the western Mediterranean Sea, *J. Mar. Syst.*, *20*(1-4), 423–442, doi:10.1016/S0924-7963(98)00078-5.
Millot, C., and I. Taupier-Letage (2005), Additional evidence of LIW entrainment across the Algerian subbasin by mesoscale eddies and not by a permanent westward flow, *Prog. Oceanogr.*, *66*(2), 231–250.
Mkhinini, N., A. L. S. Coimbra, A. Stegner, T. Arsouze, I. Taupier-Letage, and K. Béranger (2014), Long-lived mesoscale eddies in the eastern Mediterranean Sea: Analysis of 20 years of AVISO geostrophic velocities, *J. Geophys. Res. Oceans*, *119*, 8603–8626, doi:10.1002/2014JC010176.

Morán, X. A. G., I. Taupier-Letage, E. Vázquez-Dom inguez, S. Ruiz, L. Arin, P. Raimbault, and M. Estrada (2001), Physical-biological coupling in the Algerian basin (SW Mediterranean): Influence of mesoscale instabilities on the biomass and production of phytoplankton and bacterioplankton, *Deep Sea Res., Part I*, *48*(2), 405–437.

Nencioli, F., C. Dong, T. Dickey, L. Washburn, and J. C. McWilliams (2010), A vector geometry-based eddy detection algorithm and its application to a high-resolution numerical model product and high-frequency radar surface velocities in the southern California bight, *J. Atmos. Oceanic Technol.*, *27*(3), 564–579.

Nezlin, M. V., and G. G. Sutyrin (1994), Problems of simulation of large, long-lived vortices in the atmospheres of the giant planets (Jupiter, Saturn, Neptune), *Surv. Geophys.*, *15*(1), 63–99.

Obaton, D., C. Millot, G. C. d'Hières, and I. Taupier-Letage (2000), The Algerian current: Comparisons between in situ and laboratory data sets, *Deep Sea Res., Part I*, *47*(11), 2159–2190.

Pascual, A., M.-I. Pujol, G. Larnicol, P.-Y. Le Traon, and M.-H. Rio (2007), Mesoscale mapping capabilities of multisatellite altimeter missions: First results with real data in the Mediterranean Sea, *J. Mar. Syst.*, *65*(1-4), 190–211, doi:10.1016/j.jmarsys.2004.12.004.

Penven, P., V. Echevin, J. Pasapera, F. Colas, and J. Tam (2005), Average circulation, seasonal cycle, and mesoscale dynamics of the Peru current system: A modeling approach, *J. Geophys. Res.*, *110*, C10021, doi:10.1029/2005JC002945.

Puillat, I., I. Taupier-Letage, and C. Millot (2002), Algerian Eddies lifetime can near 3 years, *J. Mar. Syst.*, *31*(4), 245–259.

Pujol, M.-I., and G. Larnicol (2005), Mediterranean Sea eddy kinetic energy variability from 11 years of altimetric data, *J. Mar. Syst.*, *58*(3-4), 121–142, doi:10.1016/j.jmarsys.2005.07.005.

Renault, L., T. Oguz, A. Pascual, G. Vizoso, and J. Tintoré (2012), Surface circulation in the Alborán Sea (western Mediterranean) inferred from remotely sensed data, *J. Geophys. Res.*, *117*, C08009, doi:10.1029/2011JC007659.

Ruiz, S., J. Font, M. Emelianov, J. Isern-Fontanet, C. Millot, J. Salas, and I. Taupier-Letage (2002), Deep structure of an open sea eddy in the Algerian basin, *J. Mar. Syst.*, *33*, 179–195.

Salas, J., C. Millot, J. Font, and E. García-Ladona (2002), Analysis of mesoscale phenomena in the Algerian basin observed with drifting buoys and infrared images, *Deep Sea Res., Part I*, *49*(2), 245–266.

Stegner, A., and V. Zeitlin (1996), Asymptotic expansions and monopolar solitary Rossby vortices in barotropic and two-layer models, *Geophys. Astrophys. Fluid Dyn.*, *83*(3-4), 159–194.

Taupier-Letage, I., and C. Millot (1988), Surface circulation in the Algerian basin during 1984, *Oceanol. Acta.*, *9*, 119–131.

Taupier-Letage, I., I. Puillat, C. Millot, and P. Raimbault (2003), Biological response to mesoscale eddies in the Algerian basin, *J. Geophys. Res.*, *108*(C8), 3245, doi:10.1029/1999JC000117.

Testor, P., U. Send, J.-C. Gascard, C. Millot, I. Taupier-Letage, and K. Beranger (2005), The mean circulation of the southwestern Mediterranean Sea: Algerian gyres, *J. Geophys. Res.*, *110*, C11017, doi:10.1029/2004JC002861.

Torrence, C., and G. P. Compo (1998), A practical guide to wavelet analysis, *Bull. Am. Meteorol. Soc.*, *79*(1), 61–78.

Vandermeirsch, F., Y. Morel, and G. Sutyrin (2001), The net advective effect of a vertically sheared current on a coherent vortex, *J. Phys. Oceanogr.*, *31*(8), 2210–2225.

Vandermeirsh, F., Y. Morel, and G. Sutyrin (2002), Resistance of a coherent vortex to a vertical shear, *J. Phys. Oceanogr.*, *32*(11), 3089–3100.

Wunsch, C. (1999), Where do ocean eddy heat fluxes matter?, *J. Geophys. Res.*, *104*(C6), 13,235–13,249, doi: 199910.1029/1999JC900062.

Wyrtki, K., L. Magaard, and J. Hager (1976), Eddy energy in the oceans, *J. Geophys. Res.*, *81*(15), 2641–2646.